Journal of Energy Storage 139 (2025) 118798

Contents lists available at ScienceDirect

Journal of Energy Storage

journal homepage: www.elsevier.com/locate/est

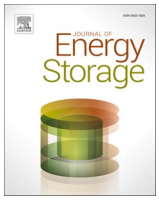

Research papers

Artificial intelligence – numerical study of a 3D model of latent heat thermal energy storage with sine-shaped fins

Obai Younis [a], Jana Shafi [b], Saeed Tiari [c], Mohammad Ghalambaz [d,e,*]

[a] Department of Mechanical Engineering, College of Engineering in Wadi Alddawasir, Prince Sattam Bin Abdulaziz University, Saudi Arabia
[b] Department of Computer Engineering and Information, College of Engineering in Wadi Alddawasir, Prince Sattam Bin Abdulaziz University, Saudi Arabia
[c] Biomedical Engineering Department, Widener University, One University Pl, Chester, PA, 19013, USA
[d] Department of Mathematical Sciences, Saveetha School of Engineering, SIMATS, Chennai, India
[e] Refrigeration and Air Conditioning Technical Engineering Department, College of Technical Engineering, The Islamic University, Najaf, Iraq

ARTICLE INFO

Keywords:
Phase change material
Artificial intelligence
Energy storage
Cavity
Melting volume fraction
Charge and discharge

ABSTRACT

As the demand for cleaner and more efficient energy solutions grows, latent heat thermal energy storage systems (LHTESSs) utilizing phase change materials (PCMs) have gained increasing attention. This study presents a numerical investigation into how different fin configurations affect the thermal performance of PCMs during melting and solidification processes in a vertical shell-and-tube LHTESS. Using a pressure-based finite-volume method and the Boussinesq approximation, three fin designs—ring, axial, and spiral—were analyzed across multiple cases. In each case, the number of fins was varied while keeping the total fin volume constant. This approach ensured a fair comparison focused purely on geometry. The artificial intelligence in the form of a deep neural network was used to provide a generalized map of the system's behavior. Among all tested configurations, the ring fin design with six fins showed the best performance, reaching a melting volume fraction (MVF) of 95.5 % at 60 min, more than double that of the no-fin baseline (45 %) and achieving 99.9 % MVF and a 28.4 % increase in stored energy rate after 100 min. The spiral fins also performed well, with a 27.8 % energy gain, while the axial fins reached a comparable 95 % MVF but delivered a slightly lower energy improvement.

1. Introduction

Thermal energy can be retained within materials through two distinct mechanisms: sensible and latent heat storage. Sensible heat storage involves raising the temperature of a solid or liquid substance to accumulate thermal energy [1]. The quantity of sensible energy stored depends on the material's temperature, specific heat capacity, and mass. In contrast, latent heat storage occurs when a material undergoes a phase transition, such as from solid to liquid, liquid to gas, or between solid phases. Phase change materials (PCMs) are specifically designed to store energy via the latent heat of fusion [2]. Among these phase transitions, the solid-to-solid transformation exhibits minimal and sluggish heat transfer, making it less effective for practical applications. Similarly, the liquid-to-gas transition is often impractical due to the excessive heat requirements, elevated temperatures, and the generation of significant gas pressure. The most viable option is the solid-to-liquid phase transition, a characteristic feature of PCMs. These materials absorb thermal energy at a nearly constant temperature as they transition from solid to liquid [3]. Subsequently, they release the stored energy at approximately the same temperature, making them highly efficient for thermal energy storage applications.

The disadvantage of phase change materials is their low thermal conductivity. This limits their use as thermal energy storage sources. For this reason, researchers have searched for various methods to increase heat transfer between phase change materials and heat transfer fluid. Thermal enhancement in latent heat thermal energy storage systems (LHTESs) is primarily achieved through two strategies. The first involves increasing the effective heat transfer surface area, commonly implemented by using finned tubes or incorporating multi-tube heat exchanger designs [4–6]. The second strategy aims to enhance the inherently low thermal conductivity of PCMs either by dispersing highly conductive particles, such as metallic nanoparticles or graphite, within the PCM [7–9].

Enhancing heat transfer using fins is a widely researched and effective approach to overcoming the inherent limitations of low thermal conductivity in PCM. *Al*-Mudhafar et al. [10] succeeded in increasing

* Corresponding author.
E-mail addresses: o.elamin@psau.edu.sa (O. Younis), j.jana@psau.edu.sa (J. Shafi), stiari@widener.edu (S. Tiari), m.ghalambaz@gmail.com (M. Ghalambaz).

https://doi.org/10.1016/j.est.2025.118798
Received 8 May 2025; Received in revised form 24 August 2025; Accepted 5 October 2025

the heat transfer of a PCM using some newly structured fins in a shell and tube LHTES. They could reduce the melting time by 33 % compared to the no-fin case. De Césaro Oliveski et al. [11] studied the effect of several fins with different areas on the melting performance of rectangular cavities using a computational fluid dynamics (CFD) approach. Furthermore, Meghari et al. [12] numerically investigated the hollow fin impact on a PCM in a spherical capsule. Shademan and Hossein Nezhad [13] simulated a vertical PCM energy storage system applying coupled boundary conditions, including different numbers of fins. They found the optimal number of fins to be 16. Moreover, Mozafari et al. [14] designed a dual LHTESS with minimum fin volume using a numerical simulation. They utilized the Response Surface Methodology (RSM) to optimize the fin angles, leading to a 7.5 % faster response. Barthwal and Rakshit [15] studied the effect of internal-external fins on the melting process of PCM using a numerical approach. They reached a maximum of 2.67 times the Nusselt number improvement.

In addition, Luo et al. [16] used the fractal fin configurations to enhance the thermal performance of PCM. They found that the PCM melting time in a combined fractal fin heat exchanger decreased by 68 % versus the traditional fractal fins. Zhao et al. [17] presented an optimized fin design for improving the thermal performance of PCM in a rectangular space. Furthermore, they derived some correlations for fin length and spacing. *Al*-Omari et al. [18] enhanced the melting rate of a heat sink filled by PCM using a numerical simulation. Their results demonstrated that the heat sink had better act on the baseline cases in a single heat sink design. Moreover, Mousavi Ajarostaghi et al. [19] numerically studied a horizontal shell/tube storage containing PCM with different fin configurations. They reduced the melting time by about 70 % when using a double vertical arrangement of fins. Triki et al. [20] numerically enhanced the thermal performance of PCMs using H-shaped fins with fractal structures. Their results showed that the phase change material's performance was improved by 69 % via a design with four fins. Additionally, Abhinand et al. [21] investigated the heat transfer rate of ice as a PCM in an LHTESS. They calculated the optimum number of fins to enhance the melting performance of ice. They also found that the increased temperature and diameter of the heat transfer fluid tube enhanced the melting rate. Li et al. [22] numerically simulated the PCM heat transfer in an LHTESS, including twisted fins. They also obtained the energy and exergy efficiencies of the double and triple fin configurations.

Several other recent studies have also been conducted regarding the positive effect of fin on improving the thermal performance of phase change materials [23–33]. For example, tree-shaped fins have been shown to reduce PCM melting time by up to 67 %, outperforming traditional fin designs like rectangular and constructal fins [23]. Additionally, the use of fins enhances natural convection, which accelerates the heat transfer process. Geometrical parameters, such as fin branching and orientation, also influence the thermal performance. A study optimizing double-branched fins found that specific configurations led to a 27.9 % improvement in PCM heat transfer efficiency [24]. Other advanced fin designs, such as L-shaped and Y-shaped fins, also contribute to better heat transmission by optimizing the dimensions and orientations [26]. These novel fin structures increase the melting and solidification rates of PCMs, thereby improving the overall efficiency of thermal energy storage systems [34]. Furthermore, the use of wave-shaped fins and other complex geometries has shown promise in enhancing heat transfer at higher rotational speeds [29]. Overall, fins significantly enhance PCM-based thermal storage systems by improving heat transfer, reducing melting times, and optimizing the performance of the PCM, contributing to more efficient energy storage solutions [32].

Although previous studies have examined a range of fin shapes and configurations, there has been little direct, side-by-side comparison of ring, axial, and spiral fin designs under identical volume constraints. The present work aims to identify the optimal fin configuration that accelerates heat transfer and maximizes efficiency while maintaining a fixed amount of fin material, ensuring cost-effectiveness and material optimization. A comprehensive numerical analysis is conducted on eleven different fin configurations, with each case designed to investigate specific aspects. The study maintains a consistent volume of fin material across all configurations, enabling a direct comparison of the thermal performance enhancements attributed to the fin modifications. This ensures that heat transfer improvements result from design optimization rather than an increase in material usage.

2. Physical model and governing equations

2.1. Model description

This study introduces a three-dimensional numerical model of a phase change material thermal storage unit to analyze the effects of different fin configurations on the melting performance of the PCM. Fig. 1 illustrates a conventional solar thermal system architecture comprising roof-mounted solar collectors and interconnected hot water storage tanks. The system operates through a closed-loop heat transfer fluid (HTF) circulation that thermally couples the solar array with the thermal storage unit. During periods of solar insolation surplus, the temperature gradient drives HTF circulation, transferring thermal energy to the water tank while simultaneously charging the LHTES unit through PCM melting. Conversely, during solar deficit conditions when domestic hot water demand occurs, the temperature differential reverses the energy flow direction - the LHTES unit discharges its stored thermal energy through PCM solidification, with the circulating HTF recovering this energy to maintain stable water tank temperatures. This bidirectional energy transfer mechanism ensures continuous thermal energy availability while optimizing solar energy utilization efficiency.

The storage unit is designed with a central hot water pipe that transfers heat to the surrounding PCM, facilitating its melting process (see Fig. 2). Although PCMs are widely used in latent heat thermal storage systems, their inherently low thermal conductivity limits heat transfer efficiency during the charging (melting) and discharging (solidification) phases. Copper fins with high thermal conductivity were employed to address this limitation. The sinusoidal fins enhance heat transfer by promoting liquid PCM' natural convection flow around them while establishing distributed contact points with the tube. Since the contact is spread along the fins, each connection between the fin and the tube supports both ends of the undulating (sine-shaped) structure. This design not only improves thermal performance but also provides mechanical stability and simplifies manufacturing.

The study examines eleven fin configurations to assess their impact on system performance. Despite the varying configurations, the total PCM and fin material (copper) volume is kept constant across all cases. This ensures that the material distribution remains uniform. The thermophysical properties of the materials used in the study are provided in Table 1. For RT35, average properties were selected for liquid/solid phases. This includes the properties of RT35 PCM (supplied by Rubitherm GmbH, Germany), which is used for thermal energy storage, copper, which is employed for the tube wall between the water and the PCM, as well as for the fins. These material properties, including density, thermal conductivity, and specific heat capacity, are essential for determining the heat transfer characteristics of the system.

To identify the effect of using fins, the result of a case without fins, named the baseline, is also prepared and presented. The baseline operates without fins and serves as a reference point for comparison. The baseline height equals 0.198 m and is considered shorter than in other cases. The height of the fin cases is equal to 0.2 m. These details are presented in Table 2. The difference in the cases' height is because of that the purpose was to have the same amount of PCM in all cases; So, by decreasing the height of the baseline, we can access the same volume amount with other fin inserted cases. Table 3 details the eleven different fin configurations. Each configuration maintains a constant total fin volume while varying the number of fins, configuration, and amplitude.

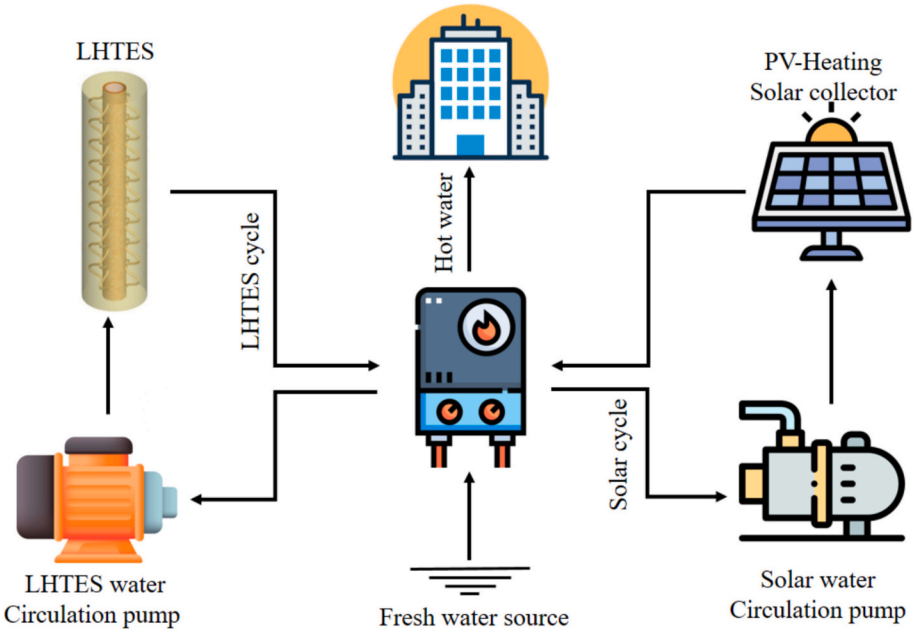

Fig. 1. A schematic diagram of the LHTES unit in a building application.

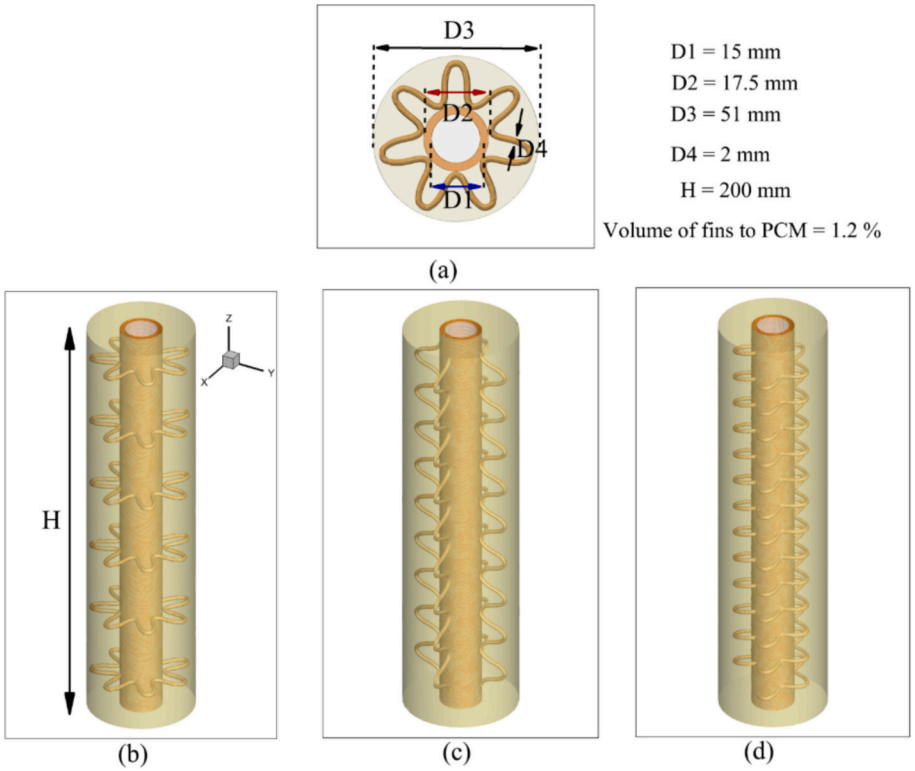

Fig. 2. A schematic view of three different fin configurations, including the geometric dimensions and sizes.

2.2. Geometrical model

The study focused on investigating the different fin shapes within the PCM container. For this purpose, three scenarios (scenarios I, II, and III) have been investigated. Each scenario consists of fins different from the fin shapes in other scenarios. In scenario I, the fins with the shape of like rings are investigated; To assess the impact of the number of fins on melting performance, four cases with different numbers of fins are evaluated (R1, R2, R3, and R4). In these cases, the number of ring fins is equal to 6, 7, 8, and 10 for R1, R2, R3, and R4, respectively. It should be noted that the volume of consumed copper for fins is constant. In this way, increasing the number of fins alters the amplitude and form of ring fins in each case. For scenario II, four cases with different numbers of axial fins from 4 to 7 fins for cases A1, A2, A3, and A4 are considered. The last scenario is related to the spiral fins with 13 and 14 fins in cases S1 and S2. Besides the number of fins, other details like fin diameter, fin volume, and the schematic of fins in each scenario are presented in Tables 3, 4, and 5. Fig. 2 shows the overall schematics of the scenarios

Table 1
The copper, water, and RT35 thermophysical properties.

Properties	Symbol	Units	RT35 [35,36]	Water [37]	Copper [38,39]
Viscosity:	μ_{PCM}	kg/m.s	0.023	0.00072	–
Density:	ρ_{PCM}	kg/m^3	820	994	8900
Specific heat:	c_p	J/kg.K	2000	4183	386
Latent heat:	L_f	J/kg	160,000	–	–
Thermal conductivity:	k	W/m.K	0.2	0.6107	380
Liquidus temperature:	$T_{PCM_{liquid}}$	K	309	–	–
Solidus temperature:	$T_{PCM_{solid}}$	K	307	–	–
Volumetric thermal expansion	β	1/K	0.0006	–	–

Table 2
Dimensions of different parts of geometries.

Cases	Water pipe diameter (m)	Tube thickness (m)	Storage tank thickness (m)	Storage tank height (m)	PCM bulk volume (m^3)
Baseline	0.015	0.00125	0.0154	0.198	0.0003385
Fin cases	0.015	0.00125	0.0154	0.2	0.0003385

and the detailed system dimensions.

2.3. Governing equations

A numerical model based on the enthalpy-porosity method is employed to analyze the melting behavior of PCM in the proposed vertical shell-and-tube LHTES. Several simplifying assumptions are applied to streamline the modeling process. The flow within the HTF and PCM region is considered incompressible, laminar, and time-dependent [40]. Effects from viscous dissipation are assumed to be negligible. The thermophysical properties of the PCM, such as density, thermal conductivity, and specific heat, are taken as constant and are not influenced by temperature changes. Natural convection in PCM region is accounted for through the Boussinesq approximation, and any volume changes resulting from phase transition are neglected for simplicity [41]. Therefore, the temperature variations in the model are limited and the phase change take place at a constant density.

The general form of the mass conservation equation for both the HTF is given by:

$$\nabla.\vec{u} = 0 \tag{1}$$

$$\rho\left(\frac{\partial\vec{u}}{\partial t} + \vec{u}.\nabla\vec{u}\right) = -\nabla p + \mu\nabla^2\vec{u} \tag{2}$$

$$\rho c_p\left(\frac{\partial T}{\partial t} + \vec{u}.\nabla T\right) = k\nabla^2 T \tag{3}$$

where $\vec{u}$ represents the velocity field. The continuity and momentum equations for the heat transfer fluid are expressed in Eqs. (1) and (2). Here, ρ denotes the fluid density, p represents pressure, and μ signifies the dynamic viscosity. The energy equation for the heat transfer fluid is presented in Eq. (3). In Eq. (3), T is the temperature field, c_P is specific heat at constant pressure, and k is the thermal conductivity. For the PCM, the following equations were applied for continuity and momentum [42,43]:

$$\nabla.\vec{u} = 0 \tag{4}$$

Table 5
Characteristics configurations of the fins for spiral cases.

Item	S1	S2
Number of fins	13	14
Fins diameter (m)	0.002	0.002
Fins volume (m^3)	3.96E-06	4.10E-06
Number of turns	11	14
Radius of the spring (cm)	13.8	13.5
Height increases per turn (cm)	16.36	12.85
Amplitude of the sine wave	4	6
Frequency of the sine wave	5	6

Table 3
A description of investigated scenarios and a pathway of the present study.

	Reference	Scenario I	Scenario II	Scenario III
Step 1: Investigate three scenarios with different numbers of fins in each of them	Baseline	R-fins case	A-fins case	S-fins case
	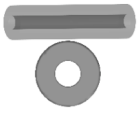		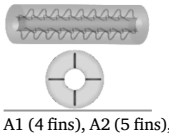	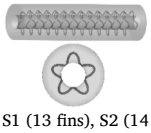
	No fins	R1 (6 fins), R2 (7 fins), R3 (8 fins), R4 (10 fins)	A1 (4 fins), A2 (5 fins), A3 (6 fins), A4 (7 fins)	S1 (13 fins), S2 (14 fins)
Step 2:	Determine a better fin configuration by comparison the best cases of each scenario and the presentation of their MVF and streamtraces contours.			
Step 3:	Present the solidification results for the best cases of the first step.			

Table 4
Characteristics configurations of the fins for horizontal and axial cases.

Investigated Cases	Types							
	Horizontal				Axial			
Item	R1	R2	R3	R4	A1	A2	A3	A4
Number of fins	6	7	8	10	4	5	6	7
Fins diameter (m)	0.002	0.002	0.002	0.002	0.002	0.002	0.002	0.002
Fins volume (m^3)	4.03E-06	4.02E-06	4.00E-06	4.04E-06	3.95E-06	4.01E-06	4.00E-06	4.08E-06

$$\rho\frac{\partial\vec{u}}{\partial t}+\rho(\vec{u}\cdot\nabla)\vec{u}=-\nabla P+\mu\left(\nabla^2\vec{u}\right)-\rho_{ref}\beta\left(T-T_{ref}\right)\vec{g}-\vec{S} \quad (5)$$

where β is the volumetric thermal expansion coefficient of liquid PCM, $\vec{g}$ is the gravitational vector which acts in downward direction only. $\vec{S}$ is the sink term for control of velocity in solid and liquid regions. The phase change of the PCM is modeled using the enthalpy-porosity technique, where the liquid fraction ϕ represents the state of the PCM (0 for solid and 1 for liquid). The Darcy sink term is introduced as [44]:

$$\vec{S}=A_{mushy}\frac{(1-\phi)^2}{\phi^3+0.001}\vec{u} \quad (6)$$

The sink term increases the resistance as the solid fraction increases, effectively becoming zero when the material is fully melted ($\phi=1$). The value of A_{mushy} needs to be chosen carefully based on experimental data or detailed numerical simulations specific to the PCM and the geometry of the LHTES system. Typically, A_{mushy} values range between 10^5 Pa·s/m^2 and 10^7 Pa·s/m^2, but the exact value can significantly influence the accuracy of the simulations, especially regarding the prediction of melting and solidification times. Here, $A_{mushy}=10^5$ Pa·s/m^2 [45–47] and the reference temperature is $T_{ref}=35$ °C. The energy equation incorporating latent heat effects in PCM is [42,43]:

$$\frac{\partial(\rho c_p T)}{\partial t}+\nabla\cdot\left(\rho c_p\vec{u}T\right)=\nabla\cdot(k\nabla T)-S_L \quad (7)$$

were the thermophysical propertices are for PCM, and S_L represents the source term due to the phase change. The source term S_L is formulated as:

$$S_L=\frac{\partial(\rho\phi L_f)}{\partial t}+\nabla\cdot\left(\rho\vec{u}\phi L_f\right) \quad (8)$$

where L_f is the latent heat of fusion. The liquid fraction parameter (ϕ) is the key indicator of the local phase state, varying from zero in the solid phase to one in the liquid phase. It is mathematically expressed using an enthalpy-based formulation.

$$\phi=\begin{cases}0 & \text{if } T<T_{\text{Solidus}}\\ \dfrac{T-T_{\text{Solidus}}}{T_{\text{Liquidus}}-T_{\text{Solidus}}} & \text{if } T_{\text{Solidus}}\le T\le T_{\text{Liquidus}}\\ 1 & \text{if } T>T_{\text{Liquidus}}\end{cases} \quad (9)$$

The melting volume fraction (*MVF*) is computed by average integration over the PCM domain as [33]:

$$MVF=\frac{\oint_V\phi dV}{\oint_V dV} \quad (10)$$

where dV is the element of volume in the PCM domain. The stored energy is computed as the sum of latent heat (Q_{latent}) in PCM domain and sensible heat ($Q_{sensible}$) energies in PCM and copper tube and fins and HTF domain as:

$$Energy\ storage=Q_{latent}+Q_{sensible} \quad (11)$$

The inlet boundary conditions specify the temperature and velocity of the incoming fluid. HTF enters the system at a temperature of $T_{\text{HTF, in}}=50$ °C for melting process and $T_{\text{HTF, in}}=20$ °C for solidification process. A velocity of $w_{\text{HTF, in}}=1.35$ cm/s. At the outlet of the HTF tube, pressure outlet boundary conditions are applied. An initial temperature of.

Walls of the container are assumed adiabatic and impermeable. The enclosure's bottom, top, and side walls are modeled with insulating, non-slip, and impermeable features, ensuring no heat or fluid movement through these surfaces. Initial conditions set the PCM to be initially solid with a uniform temperature. The initial conditions assume a cold domain with an initial temperature of $T=20$ °C for melting process and an initial temperature of $T=50$ °C for solidification process was considered. Both the velocity and pressure fields are initialized to zero.

3. Numerical method

The primary formulas were resolved utilizing ANSYS FLUENT, employing a finite volume methodology. The SIMPLE procedure was put into practice to manage the linking of pressure and velocity. Meanwhile, the QUICK approach was employed to separate the momentum and energy equations, aiming for a third order exactness in capturing the heat movement and fluid characteristics during the PCM phase alterations. The PRESTO approach was chosen to oversee pressure rectifications, proving especially advantageous for intricate, multi lobed shapes. Under relaxation components were fixed at 0.4 for pressure and velocity, 0.6 for the liquid proportion, and 1.0 for energy. Convergence benchmarks were set at 1E-4 for the continuity and momentum formulas, and 1E-6 for the energy formulas.

4. Validation and grid study

This section presents the mesh sensitivity analysis and the model validation process, which is carried out to ensure the accuracy and reliability of the numerical results. To begin with, a grid independence study was performed using the ring-fin configuration (Case R2), which features seven rows of fins. The simulations were conducted with an inlet hot water velocity of $w_{in\_HWF}=0.01345$ m/s and an inlet temperature of $T_{in\_HWF}=50^{\circ}C$. Fig. 3 (a) shows sample views of the computational mesh used for this configuration. Special attention was given to refining the grid near the heat source and around the fins, where higher gradients in temperature and velocity are expected. Three grids sizes with number of elements (*Ne*) about 500,000, 700,000, and 900,000 cells were tested to evaluate the effect of mesh resolution. As shown in Fig. 3(b), the variation in the MVF across these grids was negligible, indicating that the solution had become independent of the mesh size. Based on this, the case with 700,000-cell grid was selected for further simulations as it balanced accuracy and computational efficiency well. In addition to the mesh study, a time-step sensitivity analysis was also performed. Three-time steps (Δt), 0.15 s, 0.25 s, and 0.35 s, were tested to examine their effect on the simulation results. As illustrated in Fig. 3 (c), the differences between time steps were minimal, and a time step of 0.25 s was chosen for all simulations to ensure both stability and precision.

To verify the accuracy of the numerical model, results were compared with experimental data from previous studies on paraffin wax melting in a rectangular cavity (120 mm × 50 mm). In these experiments, all cavity walls except the left vertical wall were insulated. The wax was initially at 25 °C, while the heated wall was set to 70 °C. Temperature readings within the cavity were recorded using multiple thermocouples. Fig. 4 (a) presents a comparison of temperature distributions at four vertically aligned points within the central cavity region, comparing experimental results with simulated outcomes from this study. Additionally, Fig. 4(b) shows the stored energy and *MVF* over the melting process. The close alignment between the simulation results and experimental data validates the model's predictive capability.

5. Results and discussions

5.1. Melting volume fraction investigation

Fig. 5 depicts the *MVF* along with the energy storage per unit mass up to a simulation time of 100 min for the ring fins (R-fins) with different fin numbers of R1 to R4. All the R-fin configurations are almost close together; however, a significant enhancement in the thermal performance is obtained compared to the baseline case. At $t=60$ min, the baseline *MVF* is 0.45 while, for R1 to R4 cases, the percentage

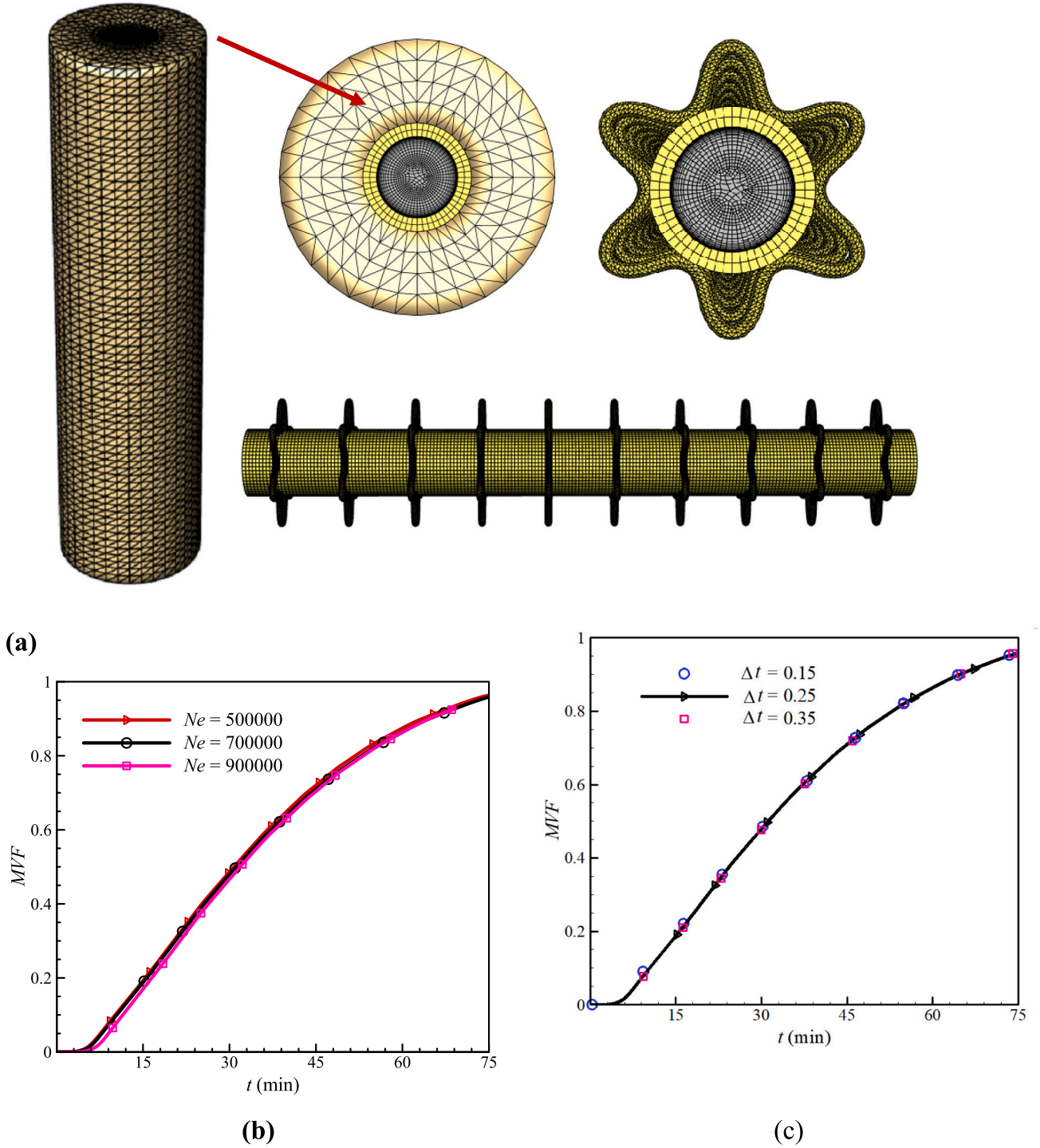

Fig. 3. The mesh study (a) Different views of LHTESs with ring fin configuration. (b) The influence of mesh size, and (c) the impact of time step on the precision of the MVF outcomes.

enhancement of *MVF* is 95.5 %, 91.8 %, 84.4 %, and 89.5 %, respectively. Furthermore, the R1 case (with 6 ring fins) reaches the maximum melting volume fraction in less time. In addition, the melting begins in the tenth minute for the baseline case, while in the other cases it starts in the fourth minute. Regarding the energy storage, two cases of R1 and R2 have the best result with an enhancement of 28.4 % compared to the baseline case at $t = 100$ min.

Fig. 6 shows the melting volume fraction along with the energy storage per unit mass up to a simulation time of 100 min for the axial fins (A-fins). An acceptable result is obtained for the *MVF* and energy storage so that the A1 case achieves the best thermal performance. However, this case's maximum *MVF* within 100 min is 95 %. At $t = 60$ min, for A1 to A3 cases, the percentage enhancement of *MVF* is 65.8 %, 63.5 %, and 43.8 %, respectively. It seems that the third case cannot compete with the other two cases. Notably, the melting process in the A-fin configurations begins earlier than in the baseline case, similar to the behavior observed with the R-fins, indicating a faster initial thermal response.

For the third scenario, the *MVF* and energy storage per unit mass up to melting time of 100 min for the spiral fins (S-fins) with two fin numbers of S1 and S2 are compared with the baseline LHTESS, as shown

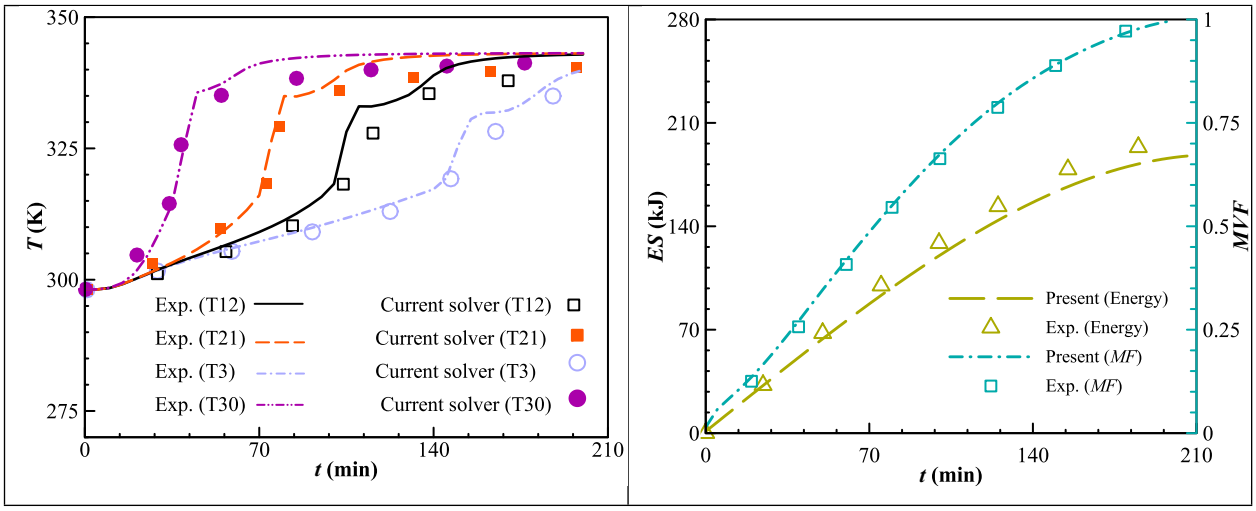

Fig. 4. A comparison between the experimental literature work and current study [48]: (a) temperature distribution, (b) stored energy, and *MVF* as a function of time.

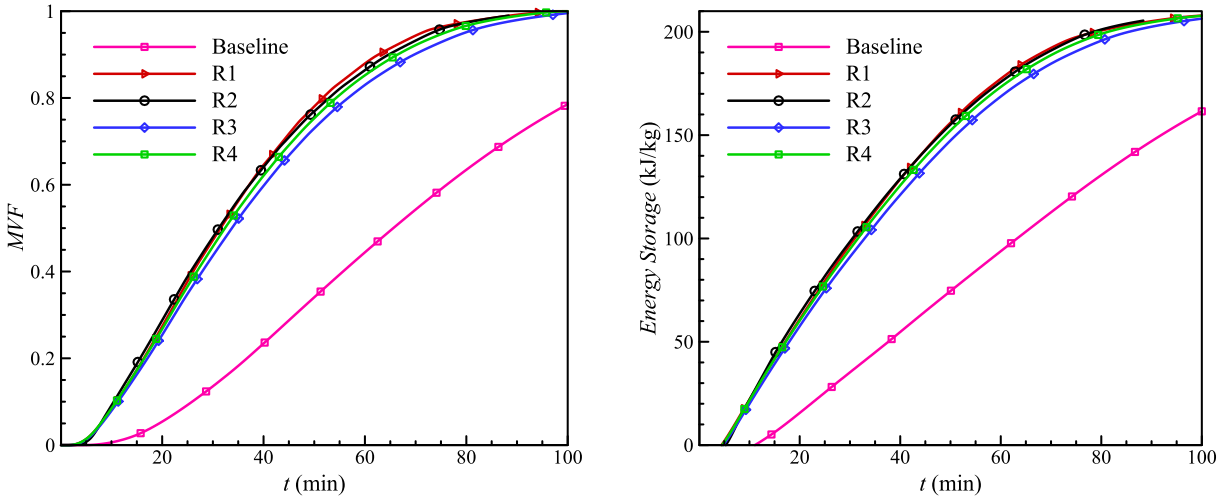

Fig. 5. *MVF* and energy storage comparison for ring fins cases.

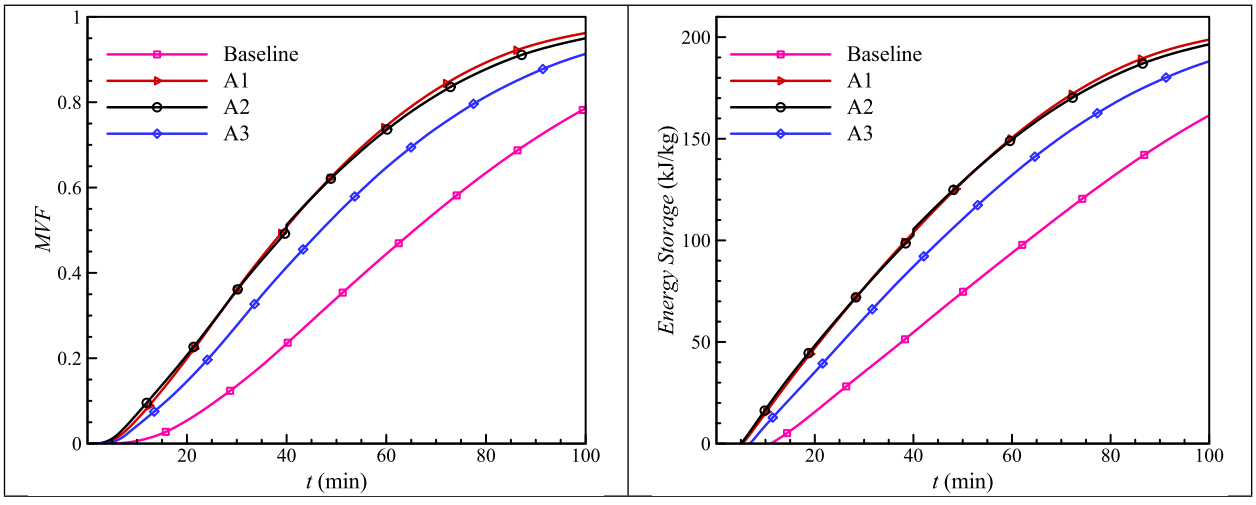

Fig. 6. MVF and energy storage comparison for axial fins cases.

in Fig. 7. Both the S1 and S2 configurations are almost close together; however, a significant enhancement in the melting rate is obtained compared to the baseline case. At $t = 60$ min, for S1 and S3 cases, the percentage enhancement of *MVF* is 89 % and 84.3 %, respectively. The S1 case (with 13 spiral fins) reaches the maximum melting volume fraction in less time. Regarding energy storage, both cases have a similar result with an enhancement of 27.8 % compared to the baseline case at $t = 100$ min.

A comparative analysis of the top-performing configurations from each fin scenario, focusing on melting rate and energy storage efficiency. Additionally, flow field characteristics—such as velocity contours and streamtraces—are examined to better understand the influence of fin geometry on natural convection within the PCM domain. To provide a complete thermal performance assessment, the discharge process (solidification phase) is also analyzed and discussed.

5.2. Comparison of the best cases of each configuration

Fig. 8 illustrates the comparison of *MVF* and energy storage for the best fin configurations in each scenario. It can be observed that the R1-fin configuration has the best performance in terms of the melting volume fraction and energy storage. Furthermore, this case reaches 99.9 % *MVF*, while the A1 case is about 95 %.

To examine how fins affect the thermal performance of the system, the contours of MVF for the best cases of R1, A1, and S1 are compared in several area sections, as depicted in Fig. 9. In all the upper sections, there is a higher melting rate due to the higher water temperature. At $t = 20$ min, the melting process is just beginning. Moreover, due to the low thermal conductivity of the PCM, no significant progress is observed in the melting of the baseline case. Analysis of the finned cases also indicated that the R1 case has the maximum thermal diffusivity compared to the others. At $t = 60$ min, the R1 and S1 cases compete closely, so a complete melting occurred in the upper four sections, while the A1 case showed poorer performance.

5.3. Flow field comparison of PCM for the best cases

One of the natural phenomena in the melting process of phase change materials is the natural upward convection flow that causes the liquid PCM to move upward. However, in finned cases, the fin structure may be such that it disrupts this upward flow. Fig. 10 shows the contours of velocity magnitude along with the streamtraces of PCM for the baseline geometry and a comparison with the best cases of R1, A1, and S1 at $t = 20$ min. In the base case, no significant melting process is yet seen due to insufficient time for heat distribution. In finned cases, the natural convection flow can pass through the space between the fins and reach the upper areas. At $t = 60$ min, as shown in Fig. 11, the convection flow forms well in the baseline case.

The A1 case can form a better upward convection flow for the finned configurations because the fins are along the flow path. However, the heat transfer distribution in this case is low. For the R1 case, reverse flow is formed around the fines. However, the convection flow is in the lower area because the upper area is completely melted due to the better structure and arrangement of the fins.

5.4. Investigating the best cases in a discharge state

In this subsection, the discharge state, for the best cases in each scenario, is investigated. Fig. 12 shows the MVF and energy storage comparisons for the best fin configurations in each scenario. Similar to the melting state, the R1-fin configuration has the best discharge state and energy storage performance. Furthermore, Fig. 13 depicts the contours of MVF for the best cases of R1, A1, and S1 are compared in several area sections. Due to the buoyancy effect and the density difference between the solid and liquid phases, the upper sections have a higher melting fraction.

6. Artificial intelligence study

Numerically simulating three-dimensional heat transfer phenomena incorporating coupled phase change dynamics and buoyancy-driven natural convection represents a formidable computational challenge. These high-fidelity Multiphysics simulations typically require extended runtime durations spanning several weeks, even when executed on state-of-the-art high-performance computing (HPC) architectures. The prohibitive computational expense associated with such detailed numerical analyses renders systematic parametric studies impractical using conventional simulation approaches, particularly when evaluating the sensitivity of PCMs' melting behavior to variations in geometric and operational parameters.

To circumvent these computational limitations while maintaining predictive accuracy, data-driven surrogate modeling techniques employing artificial neural networks (ANNs) have emerged as an effective alternative. ANNs demonstrate remarkable capability in establishing generalized input-output relationships through pattern recognition, thereby enabling rapid evaluation of system performance across diverse design configurations without repeated execution of full-scale numerical simulations. The present study implements a deep

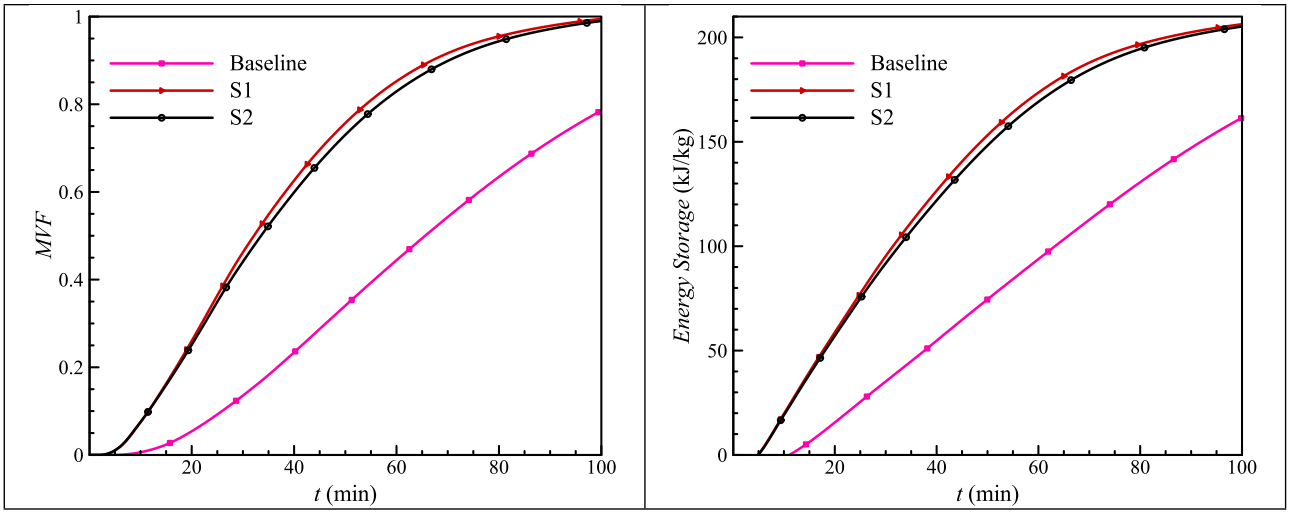

Fig. 7. *MVF* and energy storage comparison for spiral fins cases.

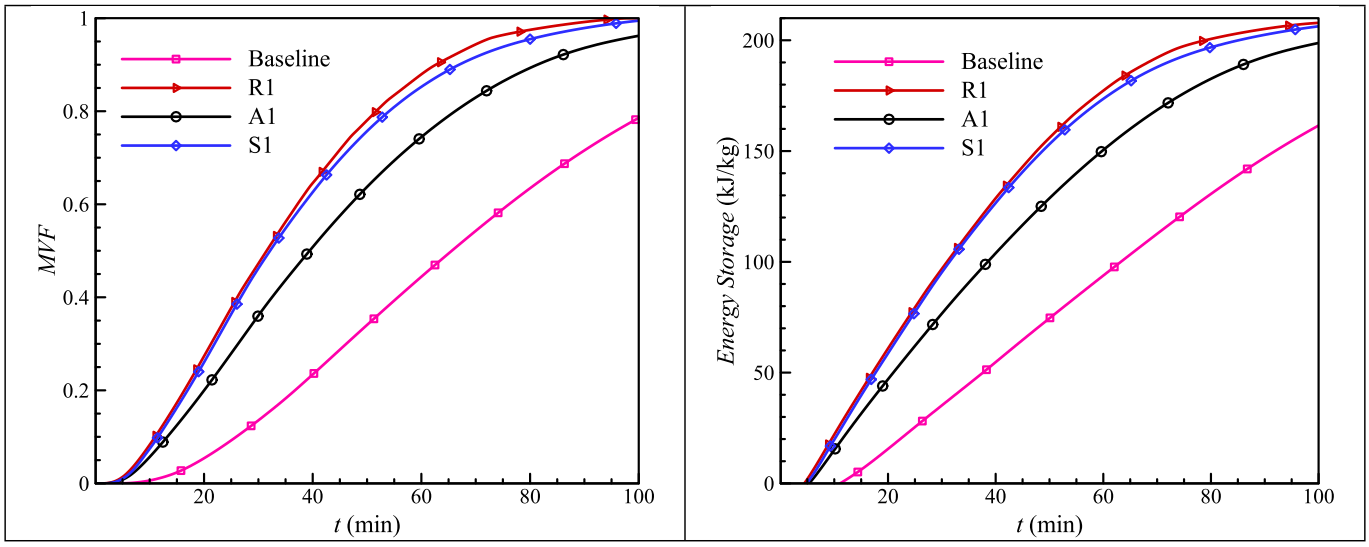

Fig. 8. *MVF* and energy storage comparison for best cases in each investigated fin configuration.

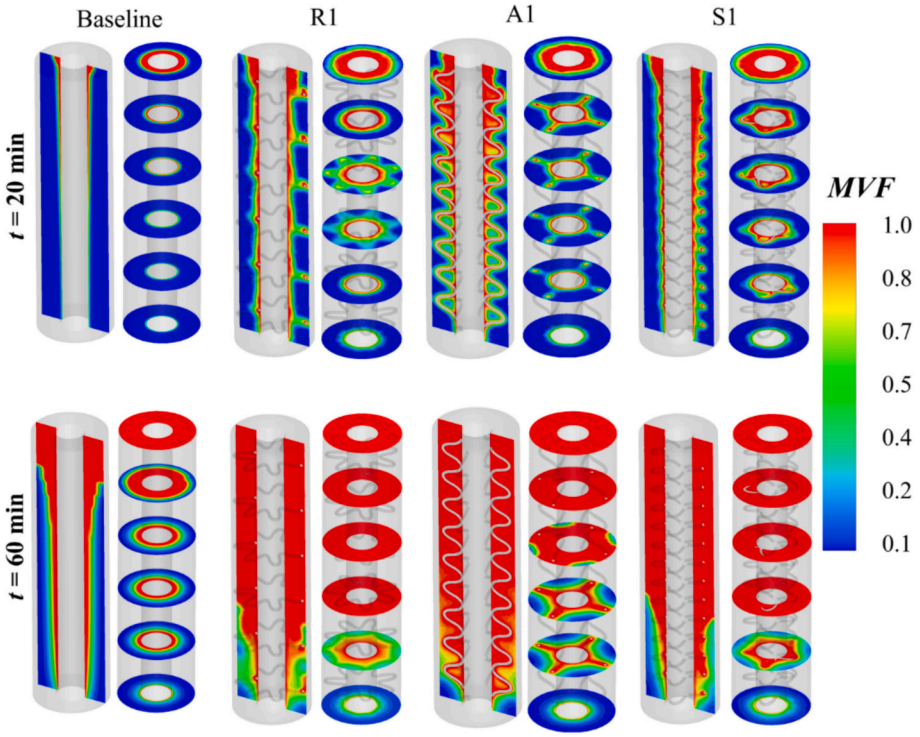

Fig. 9. *MVF* contours for best cases in each investigated fin configuration.

neural network architecture (Fig. 14) featuring: An input layer comprising three neurons corresponding to key design variables. Three fully connected hidden layers, each containing 15 neurons with nonlinear activation functions, and a single-neuron output layer providing the target thermal performance metric.

This ANN framework, illustrated schematically in Fig. 14, serves as a computationally efficient surrogate model, reducing the analytical overhead by several orders of magnitude while preserving the essential physical relationships derived from high-cost numerical simulations. The architecture was optimized through systematic hyperparameter tuning to ensure robust interpolation capabilities across the multidimensional design space.

The raw dataset was first subjected to normalization to ensure consistent scaling across input features, which is critical for the stable and efficient training of ANNs. The processed data were then fed into the ANN for supervised learning. A comprehensive dataset consisting of 24,771 sample points was utilized for training, validation, and testing. Each data point incorporates three key input parameters: Fin number – A discrete geometric parameter influencing heat transfer dynamics. Fin configuration – Categorical variable representing fin orientation (Horizontal, Axial, Spiral), and Time – Temporal evolution of the phase change process.

The corresponding output variable captures the thermal response of the system under the given conditions. To promote reproducibility and facilitate further research, the complete dataset has been made publicly available on Mendeley Data and can be accessed via the following link:

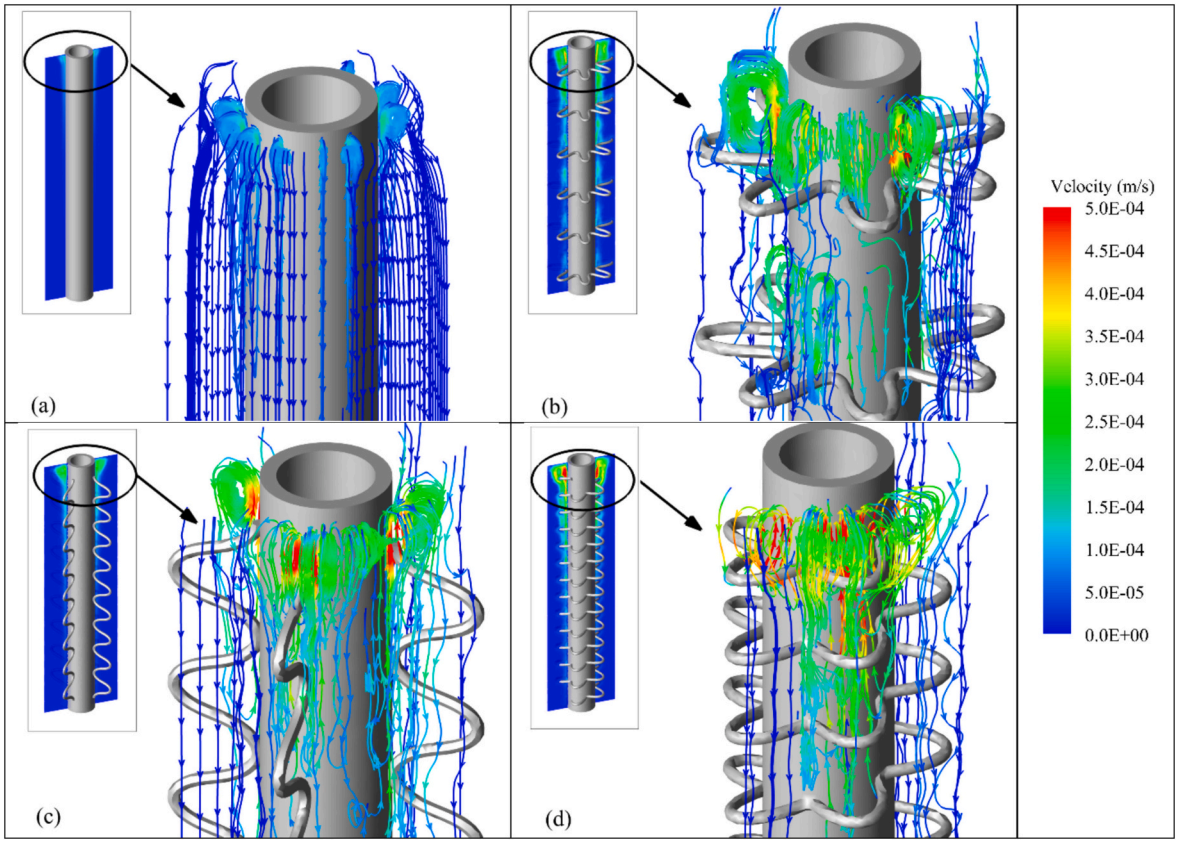

Fig. 10. Velocity contours along with streamtraces for baseline and best cases in each investigated fin configuration at $t = 20$ min, (a) Baseline, (b) R1, (c) A1, (d) S1.

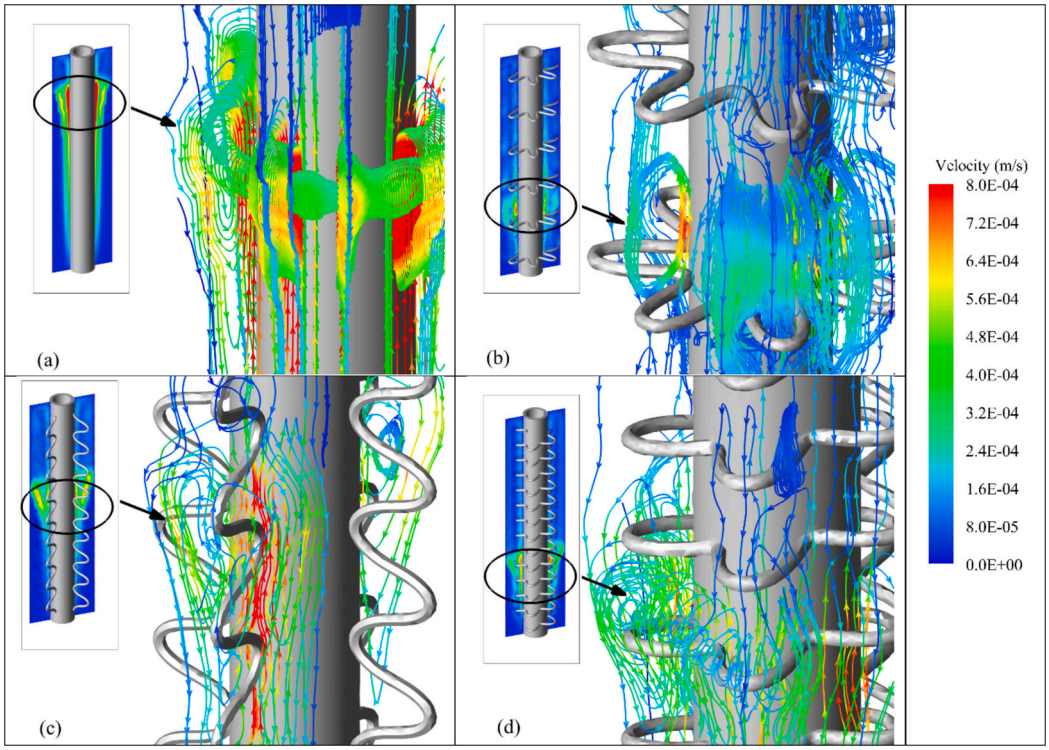

Fig. 11. Velocity contours along with streamtraces for baseline and best cases in each investigated fin configuration at $t = 60$ min, (a) Baseline, (b) R1, (c) A1, (d) S1

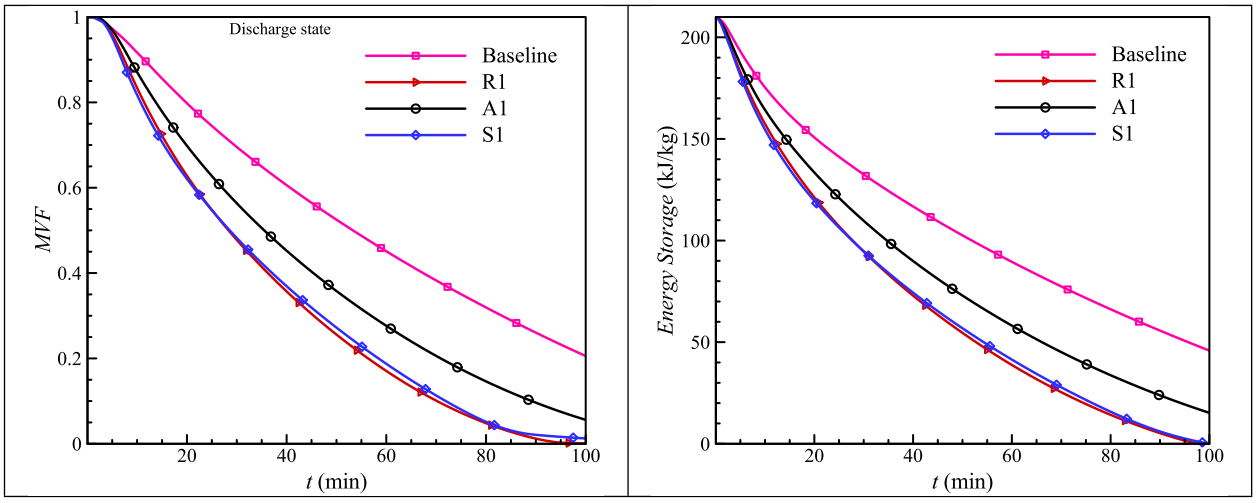

Fig. 12. Solidification and energy storage comparison for best cases in each investigated fin configuration.

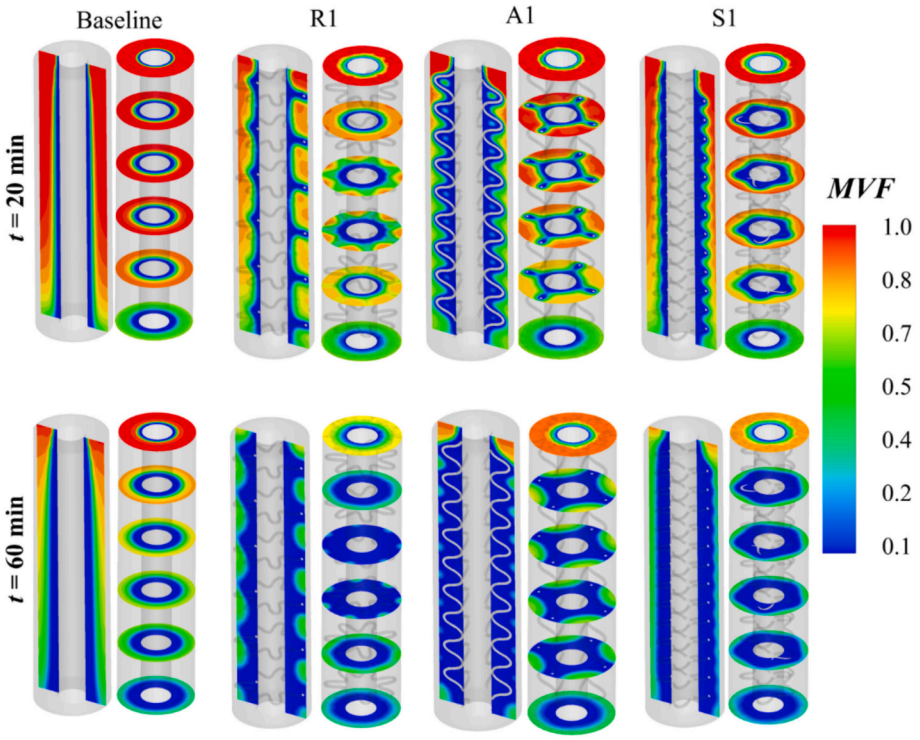

Fig. 13. MVF contours for best cases in each investigated fin configuration.

https://doi.org/10.17632/3ywfm5djfd.1

This open-access dataset enables researchers to refine existing neural network models, develop alternative machine learning approaches, or conduct more detailed post-hoc analyses. A schematic representation of the input-output structure is provided in Fig. 14.

Prior to model training, the dataset was preprocessed using the StandardScaler method [49], which standardizes features by removing the mean and scaling to unit variance. The normalization is mathematically expressed as:

$$X = \frac{x - \mu}{\sigma} \tag{12}$$

where: X = original feature value, μ = mean of the feature, σ = standard deviation of the feature. Following normalization, the dataset was randomly shuffled to eliminate any inherent ordering bias and partitioned into three subsets: 70 % (17,340 samples) for training the ANN, 15 % (3715 samples) for validation (hyperparameter tuning and early stopping), and 15 % (3715 samples) for testing (final model evaluation). This stratified division ensures robust generalization performance while mitigating overfitting.

The ANN was trained using the Adam optimizer [50], a stochastic gradient descent variant known for its adaptive learning rate properties, which enhances convergence efficiency. The training process was configured to minimize the Mean Squared Error (MSE) loss function over 1000 epochs, with a batch size of four to balance computational efficiency and gradient estimation stability. Post-training evaluation revealed exceptional model performance, as evidenced by the extremely low loss values: Validation loss = 4.85E-6 and Test loss = 5.07E-6. These negligible error metrics confirm the ANN's high predictive accuracy and its ability to generalize effectively beyond the training dataset. Fig. 15a

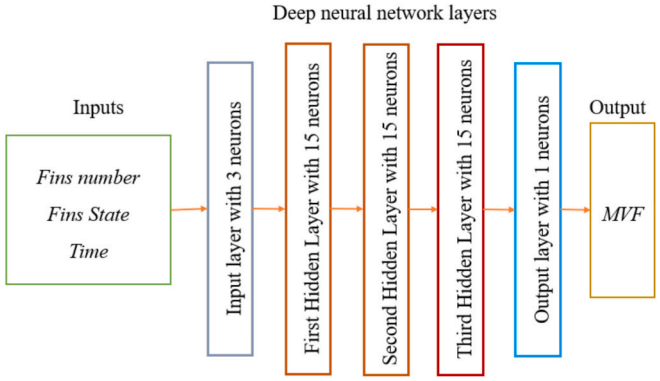

Fig. 14. The ANN structure and its inputs and outputs.

illustrates the monotonic decrease in MSE across successive training epochs for both the training and validation datasets, demonstrating stable optimization without overfitting. Fig. 15b presents a comparative analysis between the ANN's predictions and the ground-truth test data, further validating the model's precision through close alignment of forecasted and actual values. The consistent reduction in loss, coupled with the strong agreement between predicted and empirical results, underscores the robustness of the trained ANN in capturing the underlying physical relationships governing the phase-change heat transfer system.

The trained ANN was employed to generate detailed melting maps illustrating the MVF distribution across varying fin configurations, comparing horizontal (Fig. 16a) and axial (Fig. 16b) fin designs. The results demonstrate superior thermal performance of horizontal (ring) fins compared to axial fins, consistent with prior experimental and numerical findings. In ring-fin configurations, initial melting stages exhibit minimal sensitivity to fin count, as conduction dominates heat transfer and fins begin melting uniformly within their localized regions. However, as melting progresses, buoyancy-driven convection becomes increasingly influential, amplifying the impact of fin arrangement and quantity. Optimal performance was observed for ring-fin counts of 6 and 10, whereas the 8-fin configuration proved least effective, likely due to suboptimal spacing disrupting convective flow patterns.

In contrast, axial fins exhibited distinct behavior, with the 5-fin configuration achieving the shortest melting duration across all time steps. This superiority arises from a balance between conductive surface area and convective flow interference: higher fin counts reduce individual fin thickness, diminishing their penetration depth and limiting heat diffusion into the PCM's inner regions. Consequently, excessive axial fins (e.g., >5) create thermal resistance zones that impede natural convection, while insufficient fins (<5) provide inadequate conductive pathways. These insights, derived from ANN-based visualization, quantitatively validate earlier hypotheses regarding fin geometry optimization in phase-change systems, offering actionable guidelines for thermal storage design.

7. Conclusions

This study conducted a comprehensive numerical investigation into the influence of different fin configurations on the LHTESs using phase change materials. Three fin types—ring, axial, and spiral—were evaluated, each with varying fin numbers, while ensuring the total fin material volume remained constant across all cases. This approach allowed for a fair and isolated comparison of the geometric effects on thermal behavior. The ANN was successfully employed to generalize the solution and provides a wider insight into the melting behavior of the LHTES.

The results demonstrated that the inclusion of fins significantly enhanced both melting and solidification performance when compared to the baseline case without fins. Among all tested configurations, the ring fin configuration with six fins (R1 case) achieved the best overall performance. At 60 min, the R1 case reached a melting volume fraction (MVF) of 95.5 %, while the baseline case reached only 45 % in the same period. By the end of the 100-min simulation, R1 attained a nearly complete melting fraction of 99.9 % and showed a 28.4 % increase in stored energy rate compared to the baseline. The spiral fin configuration (S1) also performed well, reaching 89 % MVF at 60 min and a 27.8 %

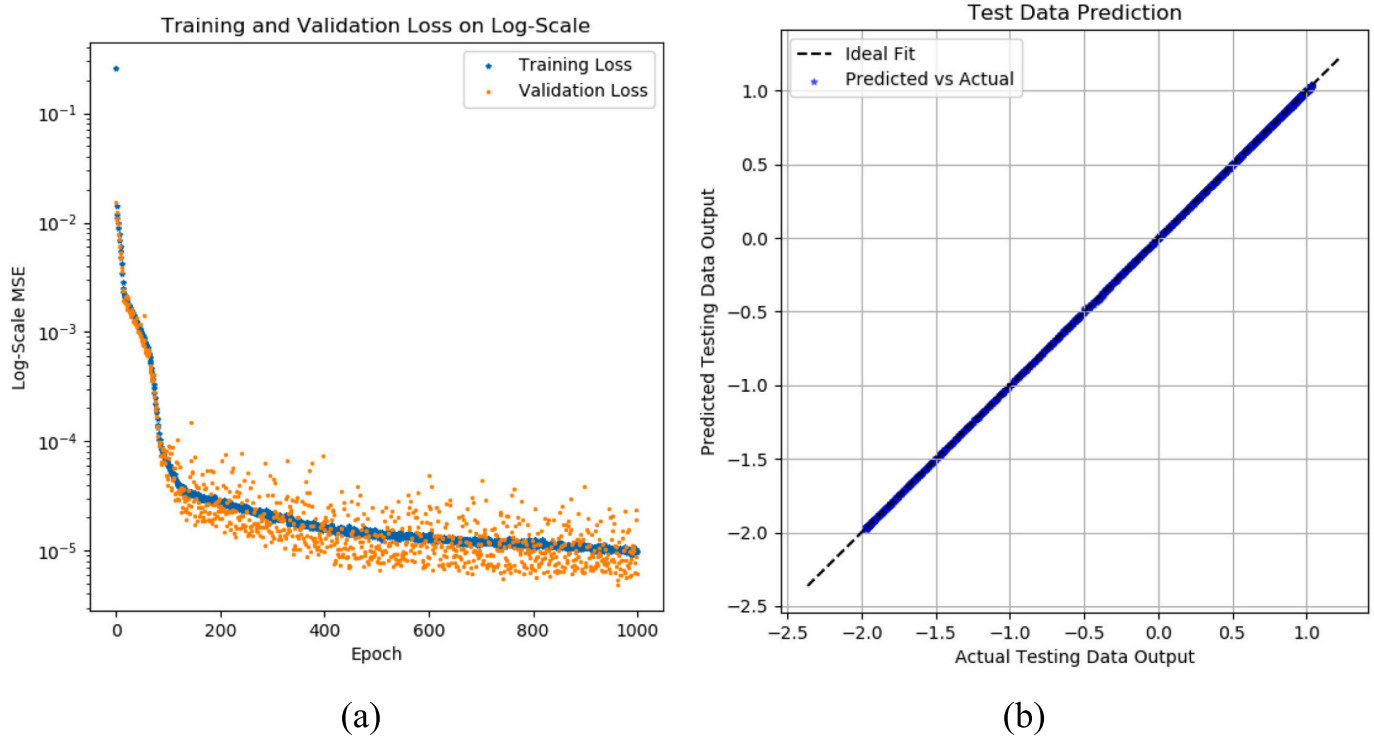

Fig. 15. The model evaluation. (a): The variation of the loss function during the training process, (b): the evaluation of ANN prediction and actual data.

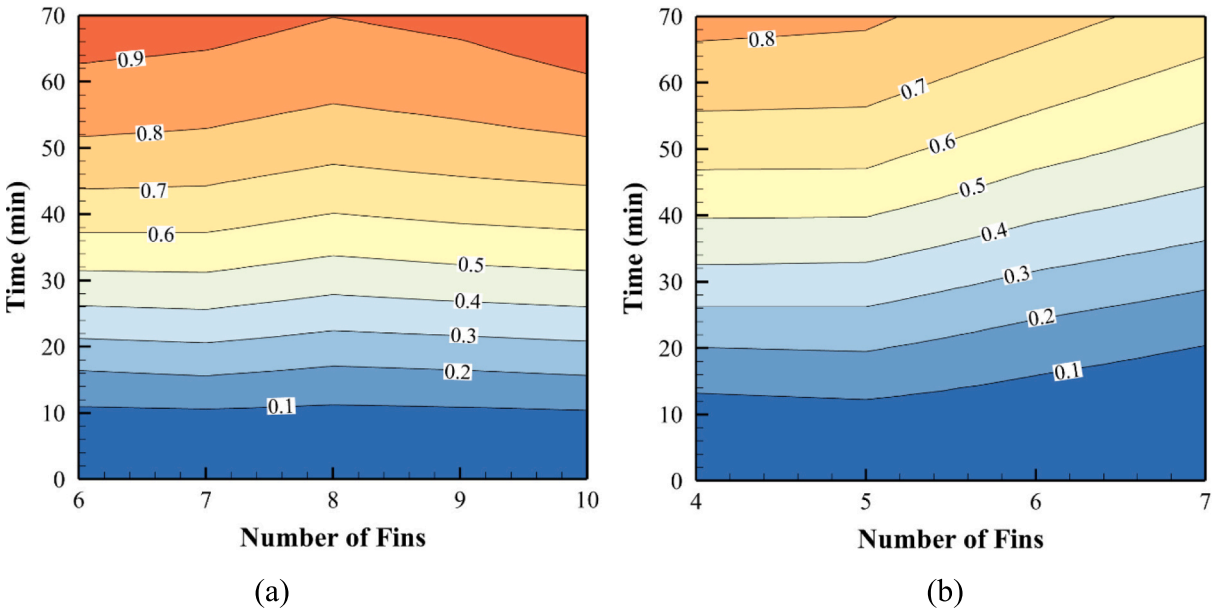

Fig. 16. The melting map of MVF for various fins for (a) the horizontal (ring) fins and (b) the axial fins configurations.

improvement in energy storage rate. Although its performance lagged slightly behind R1 in both speed and efficiency. The axial fin case (A1) achieved a respectable 95 % MVF but showed less improvement in stored energy, suggesting a more limited impact on overall heat transfer.

In addition to thermal performance, flow field analyses revealed that all fin configurations enhanced natural convection within the PCM, promoting more effective upward heat transport. The R1 configuration enabled strong convection flow in the lower regions after the upper sections had fully melted.

The ANN predictions reveal that ring fins consistently outperform axial fins in enhancing melting performance within the LHTES system. The influence of fin quantity becomes progressively more pronounced as melting advances, with natural convection playing an increasingly dominant role once a significant portion of the PCM transitions to the liquid state. For ring fin configurations, optimal performance is achieved with 6 and 10 fins, which facilitate the shortest melting durations, whereas the 8-fin arrangement demonstrates the poorest performance due to suboptimal spacing that disrupts convective flows. In contrast, among axial fin designs, the 5-fin configuration emerges as the most effective, closely followed by the 4-fin variant, as these configurations optimally balance conductive heat transfer with minimal interference to natural convection currents.

CRediT authorship contribution statement

Obai Younis: Writing – review & editing, Writing – original draft, Supervision, Project administration, Methodology, Investigation, Funding acquisition, Conceptualization. **Jana Shafi:** Writing – original draft, Software, Investigation, Formal analysis, Conceptualization. **Saeed Tiari:** Writing – review & editing, Writing – original draft, Visualization, Validation. **Mohammad Ghalambaz:** Writing – review & editing, Writing – original draft, Visualization, Validation, Software, Project administration, Methodology.

Declaration of competing interest

The authors clarify that there is no conflict of interest for report.

Acknowledgments

The authors extend their appreciation to Prince Sattam bin Abdulaziz University for funding this research work through the project number (PSAU/2024/01/31523).

Data availability

Data has been made available on Mendeley here: https://doi.org/10.17632/3ywfm5djfd.1

References

[1] A.R. Shaibani, M.M. Keshtkar, P. Talebizadeh Sardari, Thermo-economic analysis of a cold storage system in full and partial modes with two different scenarios: A case study, J Energy Storage 24 (2019).
[2] S. Sajadian, K. Hosseinzadeh, S. Akbari, A. Rahbari, P. Talebizadehsardari, A. Keshmiri, Discharge optimization in shell-and-tube latent heat storage systems using response surface methodology, Results in Engineering 25 (2025) 104157.
[3] M.A. Said, H.S.S. Aljibori, A.M. Abed, H. Togun, H.I. Mohammed, J.M. Mahdi, A. Rahbari, A.M. Sadeq, P. Talebizadehsardari, Innovative pipe profile configurations for fast charging of phase change material in compact thermal storage systems for building heating applications, Case Stud. Therm. Eng. 69 (2025) 106036.
[4] N. Modi, X. Wang, M. Negnevitsky, Experimental investigation of the effects of inclination, fin height, and perforation on the thermal performance of a longitudinal finned latent heat thermal energy storage, Energy 274 (2023).
[5] M.E. Tiji, S. Rezaei, K. Hosseinzadeh, S. Kaplan, P. Talebizadehsardari, A. Keshmiri, Optimizing heat transfer in a finned rectangular latent heat storage system using response surface methodology, Case Studies in Thermal Engineering 66 (2025) 105701.
[6] M. Esapour, A. Hamzehnezhad, A.A. Rabienataj Darzi, M. Jourabian, Melting and solidification of PCM embedded in porous metal foam in horizontal multi-tube heat storage system, Energy Convers. Manag. 171 (2018) 398–410.
[7] F.M. Azizul, A.I. Alsabery, I. Hashim, R. Roslan, H. Saleh, MHD mixed convection and heatlines approach of nanofluids in rectangular wavy enclosures with multiple solid fins, Sci. Rep. 13 (1) (2023) 9660.
[8] A. Alsabery, H. Kadhim, M. Ismael, I. Hashim, A. Chamkha, Impacts of amplitude and heat source on natural convection of hybrid nanofluids into a wavy enclosure via heatline approach, Waves Random Complex Media 33 (4) (2023) 1060–1084.
[9] N.V. Ganesh, Q.M. Al-Mdallal, G. Hirankumar, R. Kalaivanan, A.J. Chamkha, Buoyancy-driven convection of MWCNT–Casson nanofluid in a wavy enclosure with a circular barrier and parallel hot/cold fins, Alex. Eng. J. 61 (4) (2022) 3249–3264.
[10] A.H.N. Al-Mudhafar, A.F. Nowakowski, F.C.G.A. Nicolleau, Enhancing the thermal performance of PCM in a shell and tube latent heat energy storage system by utilizing innovative fins, Energy Rep. 7 (2021) 120–126.
[11] R. De Césaro Oliveski, F. Becker, L.A.O. Rocha, C. Biserni, G.E.S. Eberhardt, Design of fin structures for phase change material (PCM) melting process in rectangular cavities, J Energy Storage 35 (2021).
[12] Z. Meghari, T. Bouhal, M. Benghoulam, T.E. Rhafiki, E.M.E. Khattabi, H. doghmi, O.J. Mohammed, Numerical simulation of a phase change material in a spherical capsule with a hollow fin, J Energy Storage 43 (2021).

[13] M. Shademan, A. Hossein Nezhad, Numerical investigation of a vertical finned-tube and shell energy storage system using coupled boundary condition, J Energy Storage 41 (2021).
[14] M. Mozafari, K. Hooman, A. Lee, S. Cheng, Numerical study of a dual-PCM thermal energy storage unit with an optimized low-volume fin structure, Appl. Therm. Eng. 215 (2022).
[15] M. Barthwal, D. Rakshit, No fins attached? Numerical analysis of internal–external fins coupled PCM melting for solar applications, Appl. Therm. Eng. 215 (2022).
[16] X. Luo, J. Gu, H. Ma, Y. Xie, A. Li, J. Wang, R. Ding, Numerical study on enhanced melting heat transfer of PCM by the combined fractal fins, J Energy Storage 45 (2022).
[17] C. Zhao, J. Wang, Y. Sun, S. He, K. Hooman, Fin design optimization to enhance PCM melting rate inside a rectangular enclosure, Appl. Energy 321 (2022).
[18] S.A.B. Al-Omari, F. Mahmoud, Z.A. Qureshi, E. Elnajjar, The impact of different fin configurations and design parameters on the performance of a finned PCM heat sink, International Journal of Thermofluids 20 (2023).
[19] S.S. Mousavi Ajarostaghi, A. Amirsoleymani, M. Arıcı, A. Dolati, L. Amiri, Thermal energy storage with PCMs: A comprehensive study of horizontal shell and multi-tube systems with finned design, J Energy Storage 72 (2023).
[20] R. Triki, S. Chtourou, M. Baccar, Heat transfer enhancement of phase change materials PCMs using innovative fractal H-shaped fin configurations, J Energy Storage 73 (2023).
[21] A. S, A. Sharma, H.B. Kothadia, Performance analysis of PCM melting in a fin-assisted thermal energy storage system – A numerical study, International Communications in Heat and Mass Transfer 144 (2023).
[22] J. Li, Z.R. Abdulghani, M.N. Alghamdi, K. Sharma, H. Niyas, H. Moria, A. Arsalanloo, Effect of twisted fins on the melting performance of PCM in a latent heat thermal energy storage system in vertical and horizontal orientations: Energy and exergy analysis, Appl. Therm. Eng. 219 (2023).
[23] S.A. Marzouk, A. Aljabr, F.A. Almehmadi, M.A. Sharaf, T. Alam, D. Dobrotă, Thermal performance enhancement of phase change material melting using innovative fins, Thermal Science and Engineering Progress 61 (2025).
[24] Z. Liu, C. Li, Optimizing the geometric parameters of double branched fins for improving the melting performance of PCM, J Energy Storage 118 (2025).
[25] S.A. Shaik, P.K. Nigam, S.K. Gugulothu, Advanced fin designs for improved thermal management in PCM-based latent heat storage systems, Appl. Therm. Eng. 272 (2025).
[26] F.L. Rashid, N.S. Dhaidan, A.J. Mahdi, H.N. Azziz, R. Parveen, H. Togun, R. Z. Homod, Heat transfer enhancement of phase change materials using letters-shaped fins: A review, International Communications in Heat and Mass Transfer 159 (2024).
[27] Z. Hu, S. Jiang, Z. Sun, J. Li, Numerical simulation of fin arrangements on the melting process of PCM in a rectangular unit, Renew. Energy 220 (2024).
[28] T. Mills, K. Venkateshwar, S.H. Tasnim, S. Mahmud, Numerical and experimental investigation of the melting of a PCM in an enclosure having a tree-shaped internal fin, Thermal Science and Engineering Progress 48 (2024).
[29] A. Kumar, A. Maurya, M.I.H. Siddiqui, I.A. Alnaser, I. Ashraf, Transient analysis of PCM discharging in a rotary triplex tube with wave-shaped fins, J Energy Storage 79 (2024).
[30] H.A. Al-Salami, N.S. Dhaidan, H.H. Abbas, F.N. Al-Mousawi, R.Z. Homod, Review of PCM charging in latent heat thermal energy storage systems with fins, Thermal Science and Engineering Progress 51 (2024).
[31] H.-Y. Liu, B.-C. Qu, C.-M. Wu, Y.-R. Li, Numerical study of PCM melting performance in a rectangular container with various longitudinal fin structures, J Energy Storage 94 (2024).
[32] A. Muraleedharan Nair, C. Wilson, B. Kamkari, J. Locke, M. Jun Huang, P. Griffiths, N.J. Hewitt, Advancing Thermal Performance in PCM-Based Energy Storage: A Comparative Study with Fins, Expanded Graphite, and Combined Configurations, Energy Conversion and Management: X 23, 2024.
[33] M. Boujelbene, S.A. Mehryan, M. Sheremet, M. Shahabadi, N.B. Elbashir, M. Ghalambaz, Numerical Study of a Non-Newtonian Phase Change Flow in Finned Rectangular Enclosures, Facta Universitatis, Mechanical Engineering, Series, 2024.
[34] H.A. Al-Salami, N.S. Dhaidan, H.H. Abbas, F.N. Al-Mousawi, R.Z. Homod, Review of PCM charging in latent heat thermal energy storage systems with fins, Thermal Science and Engineering Progress 51 (2024) 102640.
[35] N.B. Khedher, H. Togun, A.M. Abed, H.I. Mohammed, J.M. Mahdi, R.K. Ibrahem, W. Yaïci, P. Talebizadehsardari, A. Keshmiri, Comprehensive analysis of melting enhancement by circular Y-shaped fins in a vertical shell-and-tube heat storage system, Engineering applications of computational fluid mechanics 17 (1) (2023) 2227682.
[36] P. Kumari, V. Saksena, R. Jha, D. Ghosh, Assessing sustainable latent heat energy storage of RT 35 phase change material in double pipe heat exchangers: A study on concentric and hairpin designs, Sustainable Chemistry for Climate Action 6 (2025) 100058.
[37] İ. Dinçer, C. Zamfirescu, Drying Phenomena: theory and Applications, John Wiley & Sons, 2016.
[38] H. Zheng, C. Wang, Q. Liu, Z. Tian, X. Fan, Thermal performance of copper foam/paraffin composite phase change material, Energy Convers. Manag. 157 (2018) 372–381.
[39] M. Bouzidi, M. Sheremet, K. Shank, S. Tiari, M. Ghalambaz, Charging and discharging heat transfer improvement of shell-tube storage utilizing a partial layer of anisotropic metal foam, J Energy Storage 79 (2024) 109948.
[40] P. Talebizadeh Sardari, G.S. Walker, M. Gillott, D. Grant, D. Giddings, Numerical modelling of phase change material melting process embedded in porous media: Effect of heat storage size, Proceedings of the Institution of Mechanical Engineers, Part A: Journal of Power and Energy 234 (3) (2019) 365–383.
[41] H. Zargartalebi, M. Ghalambaz, A. Chamkha, I. Pop, A.S. Nezhad, Fluid-structure interaction analysis of buoyancy-driven fluid and heat transfer through an enclosure with a flexible thin partition, International Journal of Numerical Methods for Heat & Fluid Flow 28 (9) (2018) 2072–2088.
[42] P. Wang, X. Wang, Y. Huang, C. Li, Z. Peng, Y. Ding, Thermal energy charging behaviour of a heat exchange device with a zigzag plate configuration containing multi-phase-change-materials (m-PCMs), Appl. Energy 142 (2015) 328–336.
[43] N.B. Khedher, K. Hosseinzadeh, A.M. Abed, K. Khosravi, J.M. Mahdi, H.S. Sultan, H.I. Mohammed, P. Talebizadehsardari, Accelerated charging of PCM in coil heat exchangers via central return tube and inlet positioning: A 3D analysis, International Communications in Heat and Mass Transfer 152 (2024) 107275.
[44] M. Esapour, M. Hosseini, A. Ranjbar, Y. Pahamli, R. Bahrampoury, Phase change in multi-tube heat exchangers, Renew. Energy 85 (2016) 1017–1025.
[45] S. Mat, A.A. Al-Abidi, K. Sopian, M.Y. Sulaiman, A.T. Mohammad, Enhance heat transfer for PCM melting in triplex tube with internal–external fins, Energy Convers. Manag. 74 (2013) 223–236.
[46] W.-B. Ye, D.-S. Zhu, N. Wang, Numerical simulation on phase-change thermal storage/release in a plate-fin unit, Appl. Therm. Eng. 31 (17) (2011) 3871–3884.
[47] E. Assis, L. Katsman, G. Ziskind, R. Letan, Numerical and experimental study of melting in a spherical shell, Int. J. Heat Mass Transf. 50 (9) (2007) 1790–1804.
[48] B. Kamkari, H. Shokouhmand, F. Bruno, Experimental investigation of the effect of inclination angle on convection-driven melting of phase change material in a rectangular enclosure, Int. J. Heat Mass Transf. 72 (2014) 186–200.
[49] Scikit-Learn, sklearn.preprocessing, StandardScaler, in: Scikit-Learn., 2023.
[50] I.K.M. Jais, A.R. Ismail, S.Q. Nisa, Adam optimization algorithm for wide and deep neural network, Knowledge Engineering and Data Science 2 (1) (2019) 41–46.